Role of pore curvature on the thermal stability of gold nanoparticles in mesoporous silica†

Mangesh T. Bore, Hien N. Pham, Timothy L. Ward and Abhaya K. Datye*

Department of Chemical and Nuclear Engineering and Ceramic and Composite Materials Center, University of New Mexico, Albuquerque NM 87131, USA. E-mail: datye@unm.edu; Fax: +1 505 277 5433; Tel: +1 505 277 0477

Pores arranged in a two-dimensional hexagonal structure inside spherical mesoporous silica particles help to prevent the thermal sintering of gold nanoparticles compared to straight pores in MCM-41.

Gold nanoparticles supported on oxide supports show high reactivity for CO oxidation at low temperature.[1] There are numerous proposals for the nature of the active site which are still being debated. A common factor in all catalysts that show high activity is the presence of Au particles in the size range of 2–5 nm. In this communication we report our initial results on the use of mesoporous silica containing uniform, ordered pores, 2 nm in diameter, to control the thermally induced coarsening of gold nanoparticles.

Mesoporous silica was prepared by two different methods. One method was based on spontaneous self-assembly of amphiphilic molecules (batch synthesis)[2] while the other is based on evaporation-induced self-assembly (aerosol synthesis).[3] Fig. 1a and Fig. 2a present the transmission electron microscope (TEM) images of the mesoporous silica particles produced by batch synthesis (MCM-41) and by aerosol synthesis (aerosol silica). The pore structure in both cases is the 2D-hexagonal structure (as confirmed by XRD, ESI†) with pore size (calculated from nitrogen adsorption isotherms with BJH theory) of 2.9 nm and 2.4 nm for the batch and aerosol synthesized mesoporous silica respectively. The major difference between these two samples is that in MCM-41, the silica pores are straight with both ends of the pore open and accessible to the gas phase. In the aerosol silica, the pores are worm-like and coiled up within the spherical silica particles. None of the pores appear to terminate on the external surface of the silica, but nonetheless the entire silica surface is accessible for N_2 adsorption, as evident from the BET surface area of 1200 m^2 g^{-1}. The internal pore structure can be seen clearly from SEM and TEM images of Pt nanowires grown within this mesoporous silica.[4]

The aerosol silica particles were produced using an ultrasonic aerosol generator. The precursor solution consisted of cetyltrimethylammonium bromide (CTAB), water, tetraethyl orthosilicate (TEOS) and 1 M hydrochloric acid. The molar ratio of TEOS : H_2O : CTAB : HCl was 1 : 63 : 0.16 : 0.02. The furnace temperature was maintained at 125 °C. The MCM-41 was prepared by using CTAB as surfactant and sodium silicate as silica source. The molar ratio of the precursor solution was $3.4SiO_2$: $1CTAB$: $286H_2O$. The powder collected was washed with water and vacuum dried. For both methods, the powder was calcined at 500 °C for 12 h in air to remove the surfactant.

To deposit gold inside the pores of mesoporous silica, we first functionalized the silica surface with an organic amine.[5,6] It is possible to mix the organic amine during the silica precipitation step, but we found this led to silica which was not well ordered. Hence, we used a two-step method, where the pre-formed silica was treated with 3-aminopropyltrimethoxysilane for 24 h, washed in DI water and vacuum dried. This amine functionalized silica powder was mixed with an aqueous hydrogen tetrachloroaurate hydrate solution (pH 7, adjusted with 1 M sodium hydroxide) to achieve a nominal gold loading of 5 wt.%. After contacting the Au precursor for 24 h, the excess was washed off with DI water and then vacuum dried for 24 h. The powder was then treated at 200 °C for 2 h in hydrogen at a ramp rate of 0.73 °C min^{-1}.

Before treatment in H_2, the Au–NH_2–MCM-41 sample shows presence of gold nanoparticles in the size range of 1 nm (see high-angle annular dark field HAADF image, ESI†). HAADF images of both Au–NH_2–MCM-41 and Au–NH_2–aerosol silica samples after H_2 treatment are shown in Fig. 1b and 2b respectively. The average gold nanoparticle size for the MCM-41 was 3.9 ± 0.9 nm while for the aerosol silica it was 1.4 ± 0.2 nm. Thus, the growth of gold nanoparticles inside the curved pores of aerosol silica was not as pronounced as that in the straight pores of the MCM-41. The gold particle size distribution is shown in Fig. 4. The particle size distribution was calculated by measuring sizes of approx. 300 particles using the software Digital Micrograph. Fig. 3 shows the X-ray diffraction patterns for both samples after the H_2 treatment. For the MCM-41, a well defined Au (111) peak can be seen in the XRD pattern while for the aerosol silica no gold peak is seen. The absence of the gold peak indicates that the gold nanoparticles are too small to detect by XRD. X-ray energy dispersive spectroscopy in the microscope confirms that both samples have a similar loading of Au (around 4.8 wt.%). We tested these reduced samples for CO oxidation with 20%CO and 10% O_2 and the balance He at a total pressure of 670 Torr (atmospheric pressure in Albuquerque).

† Electronic supplementary information (ESI) available: XRD patterns for mesoporous silica synthesized by batch and aerosol method and HAADF TEM image of gold nanoparticles supported on MCM-41 before reduction. See http://www.rsc.org/suppdata/cc/b4/b407575g/
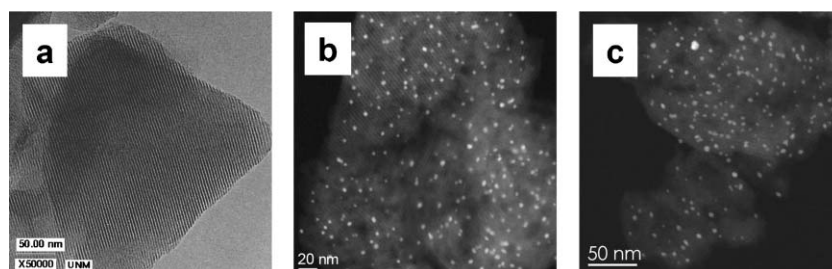
Fig. 1 (a) TEM image of MCM-41 particles; HAADF TEM images of gold nanoparticles supported on amine functionalized MCM-41 (b) after reduction, (c) after reaction.
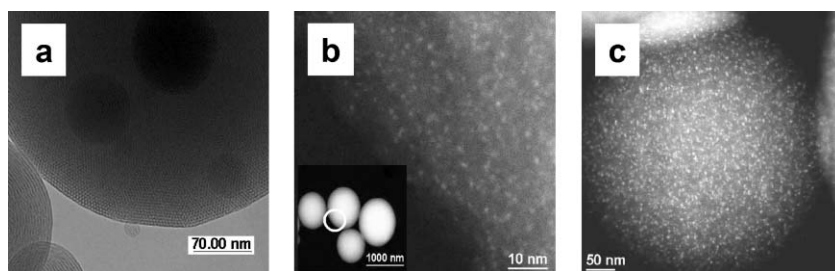
Fig. 2 (a) TEM image of aerosol silica particles; HAADF TEM images of gold nanoparticles supported on amine functionalized aerosol silica (b) after reduction, (c) after reaction.
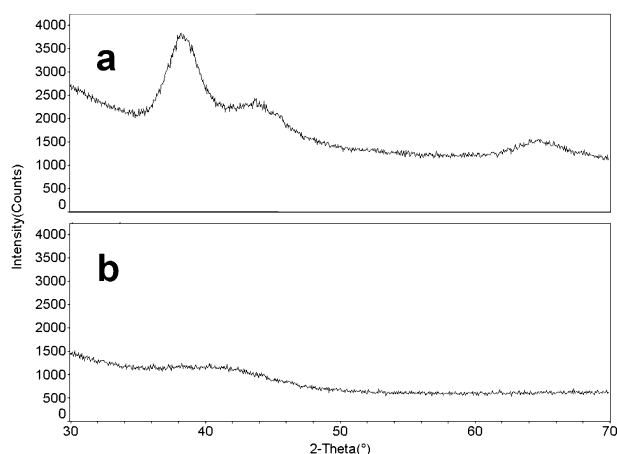
Fig. 3 XRD patterns for gold supported on mesoporous silica after reduction (a) MCM-41 (b) aerosol silica.

Fig. 4 Gold nanoparticle size distribution.

The reactivity was measured at temperatures from room temperature up to 400 °C at 50 °C intervals. These measurements were repeated for a total of *three* heating and cooling cycles indicating that the results shown here are reproducible. After reaction, the samples were removed for examination by electron microscopy. These HAADF images are labelled 'after reaction'. The reactivity at 100 °C for the gold nanoparticles supported on the MCM-41 was 0.50×10^{-5} mol s^{-1} (g catalyst)$^{-1}$ while on aerosol silica was 1.8×10^{-5} mol s^{-1} (g catalyst)$^{-1}$. The reactivity of the aerosol silica at room temperature is 0.02 mol CO_2 (mol Au)$^{-1}$ s^{-1} which after correcting for the higher CO and O_2 pressures is comparable to that reported in the literature for silica and alumina-supported Au.[7] HAADF TEM images of both Au–NH$_2$–MCM-41 and Au–NH$_2$–aerosol silica samples after reaction are shown in Fig. 1c and 2c respectively. After reaction, the average particle size was 5.9 ± 2.2 nm and 3.7 ± 0.7 nm for the MCM-41 and aerosol silica respectively.

It is apparent that the Au in the MCM-41 silica, which consists of straight pores, shows a higher degree of thermal sintering compared to the aerosol derived silica, which has wormlike pores. In both cases, the particles appear to have grown larger than the pore size. Neither the TEM images nor XRD patterns provide any evidence for destruction of the pores, since both techniques represent an average (in the case of TEM we see a projection of a 3-D structure and if one of the pores is damaged, the image will not show it). However, high resolution SEM images show that very few gold particles have come to the surface indicating the Au remains inside the pores after reaction. Thermal sintering processes involve either migration of adatoms of Au (Ostwald ripening) or migration and coalescence of the Au nanoparticles. Metal nanoparticles of the size range studied here are quite mobile even at room temperature, as shown by scanning tunnelling microscopy.[8] Regardless of the mechanism, it appears that the tortuous pore arrangements within the spherical, aerosol derived silica help to restrict the mobility, and resulting growth of the Au nanoparticles. Overbury *et al.*[9] have recently reported that Au nanoparticles within wormhole silica
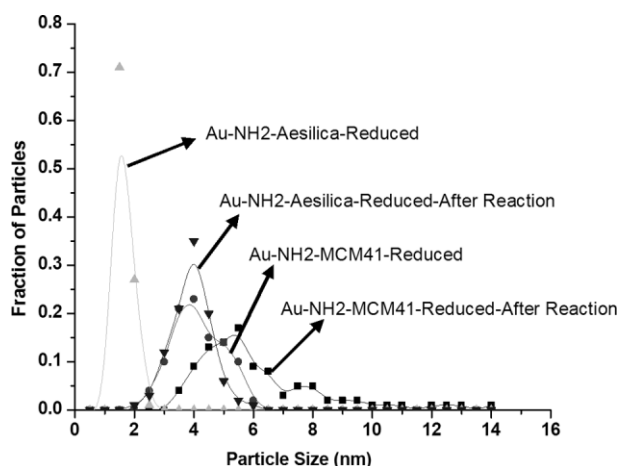
yield lower particle size after reduction at 500 °C. While similar mechanisms may be at play, the mesoporous silicas reported here with no obvious termination on the particle surface provide a novel route to prevent the thermal sintering of Au nanoparticles by retaining them within the pore structure of mesoporous silica. Despite the lack of pore termination on the silica surface, there appear to be sufficient defects in the silica, or micropores, that allow facile transport of the gas species (CO, O_2 and CO_2) into and out of the entire silica particle.

In conclusion, we have demonstrated a novel silica geometry that allows us to trap nanoparticles, and restrict the mobility of species that lead to thermal sintering. The silica shells help to contain the nanoparticles within the pore structure, and protect the active phase from gas phase poisons, while allowing facile access to gas phase species.

Notes and references

1 M. Haruta, S. Tsubota, T. Kobayashi, H. Kageyama, M. J. Genet and B. Delmon, *J. Catal.*, 1993, **144**, 175.
2 C. T. Kresge, M. E. Leonowicz, W. J. Roth, J. C. Vartuli and J. S. Beck, *Nature*, 1992, **359**, 710.
3 M. T. Bore, S. B. Rathod, T. L. Ward and A. K. Datye, *Langmuir*, 2003, **19**, 256.
4 M. T. Bore, T. L. Ward, A. Fukuoka and A. K. Datye, *Catal. Lett.*, in press.
5 A. Gosh, C. R. Patra, P. Mukherjee, M. Sastry and R. Kumar, *Microporous Mesoporous Mater.*, 2003, **58**, 201.
6 H. Zhu, B. Lee, S. Dai and S. H. Overbury, *Langmuir*, 2003, **19**, 3974.
7 M. Okumura, S. Nakamura, S. Tsubota, T. Nakamura, M. Azuma and M. Haruta, *Catal. Lett.*, 1998, **51**, 53.
8 L. M. Sanders, PhD Thesis, University of New Mexico, Albuquerque, NM, 2003.
9 S. H. Overbury, L. Ortiz-Soto, H. Zhu, B. Lee, M. D. Amiridis and S. Dai, *Catal. Lett.*, 2004, **95**, 99.